Lifetime of angular momentum in a rotating strongly interacting Fermi gas

S. Riedl,[1,2] E. R. Sánchez Guajardo,[1,2] C. Kohstall,[1,2] J. Hecker Denschlag,[1] and R. Grimm[1,2]

[1]*Institut für Experimentalphysik und Zentrum für Quantenphysik, Universität Innsbruck, 6020 Innsbruck, Austria*
[2]*Institut für Quantenoptik und Quanteninformation,*
Österreichische Akademie der Wissenschaften, 6020 Innsbruck, Austria
(Dated: November 20, 2018)

We investigate the lifetime of angular momentum in an ultracold strongly interacting Fermi gas, confined in a trap with controllable ellipticity. To determine the angular momentum we measure the precession of the radial quadrupole mode. We find that in the vicinity of a Feshbach resonance the deeply hydrodynamic behavior in the normal phase leads to a very long lifetime of the angular momentum. Furthermore, we examine the dependence of the decay rate of the angular momentum on the ellipticity of the trapping potential and the interaction strength. The results are in general agreement with the theoretically expected behavior for a Boltzmann gas.

I. INTRODUCTION

The dynamics of an ultracold quantum gas is an important source of information on the physical nature of the system. A particularly interesting situation is an atomic Fermi gas in the vicinity of a Feshbach resonance [1, 2]. The Feshbach resonance allows us to tune the two-body interaction and thus to control the coupling between the atoms. It connects a molecular Bose-Einstein condensate (BEC) with a Bardeen-Cooper-Schrieffer (BCS) superfluid. In the crossover region between these two limiting cases the center of the Feshbach resonance is of special interest. Here the unitarity-limited interactions lead to universal behavior of the Fermi gas.

The strong two-body interactions close to the Feshbach resonance lead to very low viscosity and hydrodynamic behavior in the normal phase, similar to properties of a superfluid [3, 4]. The coexistence of normal and superfluid hydrodynamic behavior is a special property of the strongly interacting Fermi gas, which stands in contrast to ultracold Bose gases, where deep hydrodynamic behavior is usually restricted to the superfluid condensate fraction. The low-viscosity hydrodynamic behavior leads to a long lifetime of collective motion in the system. Using collective modes the dynamics has been investigated in a broad range of temperatures and interaction strengths in the crossover region [3, 4, 5, 6, 7, 8, 9, 10, 11], including the hydrodynamic regime in the normal phase. Another important collective motion is the rotation of the gas, which is of particular interest in relation to superfluidity [12].

In this Article, we study the lifetime of the angular momentum of a rotating strongly interacting Fermi gas. We determine the angular momentum using the precession of the radial quadrupole mode. This method is well established to study the angular momentum in experiments with BEC [13, 14, 15]. We observe that the unique hydrodynamic behavior of the strongly interacting Fermi gas leads to particularly long lifetimes of the angular momentum. We perform a quantitative analysis of the dissipation of the angular momentum caused by the trap anisotropy for a gas in the unitarity limit. The measurements show general agreement with the expected behavior for a Boltzmann gas [16]. As shown in a previous study comparing experiment and theory [11], a Boltzmann gas describes the behavior of a gas in the normal state with unitarity-limited interactions reasonably well. Finally we study the dependence of the lifetime on the interaction strength of the gas in the crossover region between the BEC and BCS regime.

II. EXPERIMENTAL PROCEDURE

To realize an ultracold strongly interacting Fermi gas we trap and cool an equal mixture of ^{6}Li atoms in the lowest two atomic states as described in our previous work [10, 17]. We control the interparticle interaction by changing the external magnetic field in the vicinity of a broad Feshbach resonance centered at $834\,\text{G}$ [18]. The atoms are held by an optical dipole trap using a red-detuned, single focused laser beam and an additional magnetic trap along the beam; this magnetic confinement dominates over the optical confinement along the beam under the conditions of the present experiments. The resulting trap provides weak confinement along the beam (z axis) and stronger transverse confinement (x-y plane), leading to a cigar-shaped cloud. The trap is well approximated by a harmonic potential with trap frequencies $\omega_x \approx \omega_y \approx 2\pi \times 800\,\text{Hz}$ and $\omega_z = 2\pi \times 25\,\text{Hz}$. The trap in general also has a small transverse ellipticity, which can be controlled during the experiments. We define an average transverse trap frequency as $\omega_r = \sqrt{\omega_x \omega_y}$. The Fermi energy of the noninteracting gas is given by $E_F = \hbar(3N\omega_x\omega_y\omega_z)^{1/3} = \hbar^2 k_F^2/2M$ where $N = 5 \times 10^5$ is the total atom number, M is the atomic mass and k_F is the Fermi wave number. The corresponding Fermi temperature is $T_F = E_F/k = 1.3\,\mu\text{K}$, with k the Boltzmann constant. The interaction strength is characterized by the dimensionless parameter $1/k_F a$, where a is the atomic s-wave scattering length.

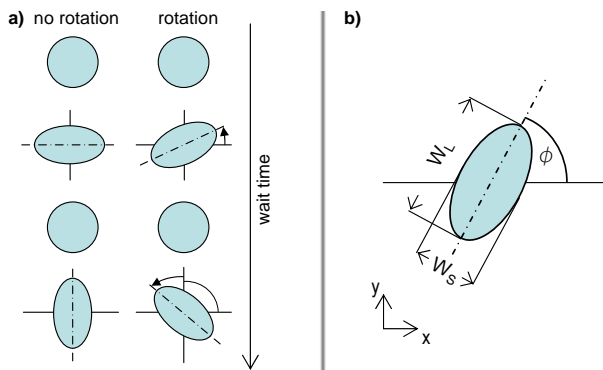To dynamically control the shape of the trapping po-

Figure 1: Oscillation of the cloud after excitation of the radial quadrupole mode. For a rotating hydrodynamic gas the principal axes of the quadrupole mode oscillation precess with a frequency determined by the angular momentum of the gas. To follow the precession we measure the angle of the long axis of the cloud. Note that every half oscillation period this angle changes by $\pi/2$ because of the mode oscillation; see also Fig. 2. The oscillation of the cloud shape is determined by measuring the widths along the short (W_S) and the long axis (W_L) of the cloud.

tential in the transverse plane we use a rapid spatial modulation of the trapping laser beam by two acousto-optical deflectors, which allows us to create time-averaged trapping potentials [10]. The control over the potential shape has two different applications for the measurements. As a first application we use it to adjust the static ellipticity $\epsilon = (\omega_x^2 - \omega_y^2)/(\omega_x^2 + \omega_y^2)$ of the trap in the x-y plane. This allows us to compensate for residual ellipticity of the trapping potential, i.e. of the trapping laser beam, and also to induce a well defined ellipticity. The second application is the creation of a rotating elliptic potential with a constant ellipticity ϵ' [19]. This is needed to spin up the gas. Both the static ellipticity in the x-y plane and the rotating elliptic potential can be controlled independently. To determine the ellipticity we measure the frequency of the sloshing mode along the two principal axes of the elliptic potential. This allows controlling the ellipticity with an accuracy down to typically 0.005.

To measure the angular momentum of the cloud we exploit the fact that collective excitation modes are sensitive to the rotation of the cloud. Here we use the precession of the radial quadrupole mode to determine the angular momentum of the rotating cloud; see Fig. 1. This method works under the general condition that the gas behaves hydrodynamically [20]. In our case of a strongly interacting Fermi gas, this method probes both the superfluid and the classically hydrodynamic part and does not distinguish between these two components. For the case of atomic BEC, the precession has been well studied in theory [21, 22, 23, 24] and used in experiments to determine the angular momentum of the BEC [13, 14, 15]. For an atomic BEC the non-condensed part is usually collisionless and does not contribute to the mode precession.
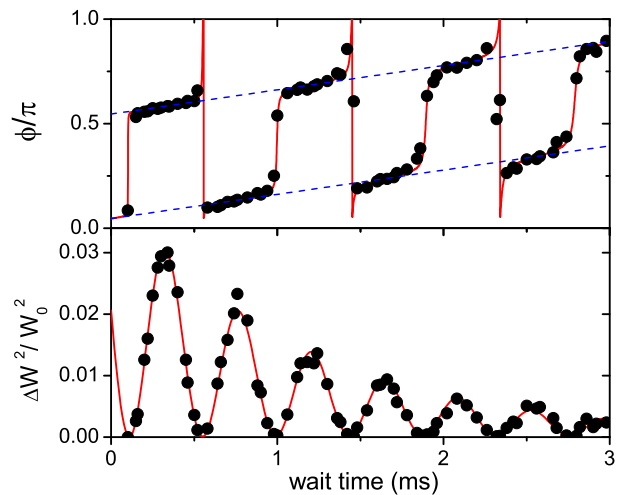

Figure 2: Evolution of the quadrupole mode in a rotating Fermi gas in the unitarity limit. The upper panel shows the precession of the principal axes of the mode. The experimental data are shown by the dots. The solid line represents a fit according to Eq. A1. The dashed lines correspond to the idealized precession of the angle when there is no damping present in the mode. Whenever the oscillation of the difference in widths $\Delta W^2/W_0^2$ (lower panel) has a local maximum the observed precession angle coincides with the idealized precession. The parameter W_0 is the average width of the cloud. The finite value of ϕ at zero wait time results from the precession of the cloud during expansion. Here $L_z = 1.7\hbar$ and $T/T_F \approx 0.2$.

The radial quadrupole mode consists of two collective excitations with angular quantum numbers $m = +2$ and $m = -2$ and frequencies ω_+ and ω_-, respectively. These two excitations correspond to an elliptic deformation of the cloud rotating in opposite directions. The superposition of the excitations results in the radial quadrupole mode. For a gas at rest the two excitations are degenerate, while for a gas carrying angular momentum the frequencies are different, which causes a precession of the mode, see Fig. 1. The mode precesses with a frequency $\Omega_\phi = (\omega_+ - \omega_-)/4$. The angular momentum itself can be calculated from the precession frequency [24] using

$$\Omega_\phi = L_z/(2Mr_{\rm rms}^2). \qquad (1)$$

Here L_z is the average angular momentum per atom and $r_{\rm rms}^2$ is the mean value of $x^2 + y^2$ of the density distribution [25].

To excite the quadrupole mode we switch on an elliptic potential for $50\,\mu$s; this short elliptic deformation does not affect the angular momentum of the gas. For the excitation we make sure that ω_r does not change. This ensures that no compression mode is excited and only an equal superposition of the $m = \pm 2$ modes is created [10].

To follow the quadrupole oscillation we determine the angle of the long axis, ϕ, and the difference of the widths along the principle axes of the cloud, $\Delta W = W_L - W_S$, after a variable wait time in the trap; see Fig. 1. There-

fore we fit a zero temperature, two-dimensional Thomas-Fermi profile to absorption images [26]. We also keep the angle of the long axis a free fit parameter. The width of the cloud is defined as twice the Thomas-Fermi radius.

To resolve the density distribution in the x-y plane we let the cloud expand for $0.8\,\mathrm{ms}$ before taking the image. The expansion does not only increase the width of the cloud but also leads to an increase of the precession angle as a consequence of the angular momentum. A quantitative analysis of the small contribution to the total precession angle that results from the expansion is given in Appendix B.

Figure 2 shows the evolution of the precessing quadrupole mode. The upper part shows the precession angle. The finite value of ϕ at zero wait time results from the expansion. The periodic jumps of the precession angle reflect the alternation between the long and the short axis while the quadrupole mode evolves. As the precession proceeds, these jumps become more and more smooth. This is caused by stronger damping of the $m = -2$ excitation compared to the $m = +2$ excitation. Similar behavior has been observed in Ref. [27] for the case of a BEC. There the authors discuss two possible mechanisms where the difference in damping is either due to a rotating thermal cloud [28] or Kelvin mode excitations [20]. From our measurements we cannot discriminate between these two mechanisms.

To fit the observed precession of the quadrupole mode we use the function given in Appendix A. We find very good agreement between the data and the expected behavior. For the data set shown in Fig. 2 the angular momentum is $1.7\hbar$. The average damping rate is $(\Gamma_- + \Gamma_+)/2 = (460 \pm 30)\,\mathrm{s}^{-1}$, while the difference in the damping rate of the $m = -2$ compared to the $m = +2$ excitation is $\Gamma_- - \Gamma_+ = (80 \pm 40)\,\mathrm{s}^{-1}$.

We find that a simplified procedure can be used to determine the angular momentum from a single measurement, instead of fitting the whole precession curve. If the measurement is taken at a time when ΔW^2 has a local maximum, the precession angle ϕ is independent of the distortion caused by the difference in the damping rates between the two excitations; see Fig. 2. This allows us to determine the difference $\omega_+ - \omega_- = 4\,\phi/\Delta t$ and therefore to determine L_z with a single measurement. The duration Δt is the sum of the wait time in the trap and an effective precession time t_e, which accounts for the precession of the quadrupole mode during expansion as discussed in Appendix B. Depending on the damping of the mode oscillation we measure the precession angle at the first or second maximum of ΔW^2 [29].

To determine the temperature of the gas in the unitarity limit we first adiabatically change the magnetic field to $1132\,\mathrm{G}$ [30], where $1/k_F a \approx -1$, to reduce the effect of interactions on the density distribution [31]. Under this condition, for $T > 0.2 T_F$, the interaction effect on the density distribution is sufficiently weak to treat the gas as a noninteracting one and to determine the temperature from time-of-flight images. We fit the den-
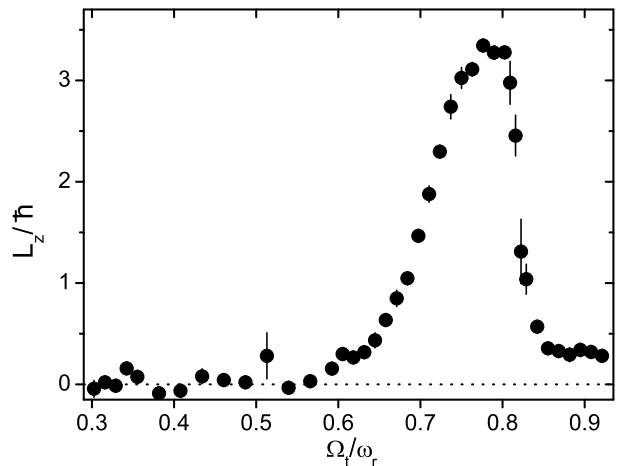

Figure 3: The angular momentum L_z as a function of the rotation frequency Ω_t of the elliptic trap. Here we spin up the gas for $t_{\mathrm{rot}} = 60\,\mathrm{ms}$. The temperature is $T/T_F \approx 0.2$. The gas is in the unitarity limit.

sity distribution after $2\,\mathrm{ms}$ release from the trap to a finite-temperature Thomas–Fermi profile. The temperature measured at $1132\,\mathrm{G}$ is converted to the temperature in the unitarity limit under the assumption that the conversion takes place isentropically, following the approach of Ref. [32].

III. SPINNING UP THE GAS

To spin up the gas we introduce a rotating anisotropy into the initially round trap in the x-y plane. More specifically, we suddenly switch to a rotating elliptic trap potential with a rotation frequency Ω_t and ellipticity $\epsilon' = 0.03$, rotate for a time t_{rot} on the order of $100\,\mathrm{ms}$, and then ramp down the ellipticity in $50\,\mathrm{ms}$ while the trap is still rotating.

In the case of hydrodynamic behavior of the gas this spinning up method is resonantly enhanced in a certain range of rotation frequencies; see Fig. 3. The reason for this behavior is the resonant excitation of quadrupolar flow which leads to a dynamic instability when Ω_t is close to half the oscillation frequency of the radial quadrupole mode $\omega_q/2 = 0.71\,\omega_r$. This effect was used to nucleate vortices in a BEC [33] and was further studied in Refs. [34, 35]. A signature of the resonant excitation is a strong elliptic deformation of the cloud shape which exceeds the ellipticity of the trap ϵ' during the spin-up process. We clearly see this effect when we spin up the gas. We also find that the rotation frequency where L_z starts to increase strongly depends on ϵ' and t_{rot} in a similar way as it was observed in Refs. [34, 35]. Note that we cannot draw any conclusion concerning superfluidity from the resonant behavior of L_z in Fig. 3 because it is only a consequence of hydrodynamic behavior and the strongly interacting gas is hydrodynamic both below and

above T_c. In fact, for temperatures clearly above T_c we find similar behavior for L_z as a function of Ω_t.

For an atomic BEC, L_z was found to first increase abruptly from 0 to $1\hbar$ with Ω_t, caused by the appearance of a centered vortex [13]. As the formation of pairs is necessary for superfluidity in the BEC-BCS crossover regime, the angular momentum per atom of a single vortex in the center of the cloud amounts to $L_z = \hbar/2$. We do not observe such an abrupt increase of L_z. Nevertheless this does not exclude that vortices are created during our spin-up process; the abrupt change of L_z is not a necessary consequence of the creation of vortices as the angular momentum of a vortex depends on its position in an inhomogeneous gas [13]. Furthermore our measurement of L_z cannot distinguish between the angular momentum carried by the superfluid and the normal part of the cloud. Also we cannot directly observe vortices in our absorption images; we believe that the reason is the very elongated cloud which strongly decreases the contrast of the vortex core in the absorption images.

During our spin-up process we observe a significant heating of the gas depending on the rotation frequency and the rotation time. We keep these two parameters as small as possible. We find that a rotation frequency of $\Omega_t/\omega_r = 0.6$ and $t_{\rm rot} = 200\,$ms lead to an angular momentum of about $L_z = 2\hbar$. This is sufficient to perform the measurements, and at the same time does only moderately increase the temperature.

We determine the temperature of the gas after the spin-up process. To avoid complications in the temperature measurement we wait until the rotation has completely decayed. To keep this wait time short, on the order of $100\,$ms, we speed up the decay by increasing the ellipticity of the trap; see discussion below. Note that the low initial angular momentum used in the experiments, always staying below $3\hbar$, does not lead to a significant increase in the temperature when the rotation energy is completely converted into heat [36].

IV. LIFETIME OF THE ANGULAR MOMENTUM

In an elliptic trap the angular momentum is not a conserved quantity and hence can decay. The dissipation of L_z is due to friction of the gas caused by the trap anisotropy. Here we investigate the dependence of the decay of L_z on the static ellipticity for the case of unitarity-limited interactions. We compare our experimental results to the predicted behavior for a rotating Boltzmann gas [16]. Finally we study the dependence of the decay rate on the interaction strength in the BEC-BCS crossover regime.

The fact that the gas consists of two different components, the normal and the superfluid part, leads in general to a complex behavior for the decay of L_z. For example, in the case of a BEC an exponential decay is related to the co-rotation of the thermal cloud with the
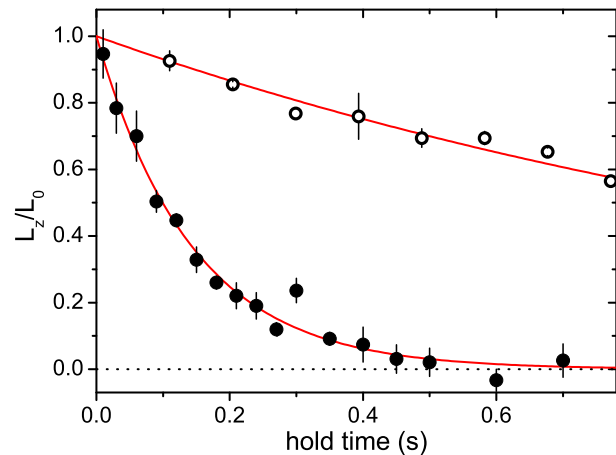

Figure 4: Decay of the angular momentum L_z for a gas in the unitarity limit. The temperature is $T/T_F = 0.22(3)$. We fit an exponential decay behavior (solid lines) to the experimental data points. For low ellipticity $\epsilon = 0.009$ (open dots) the lifetime is $1.4\,$s, while at higher ellipticity $\epsilon = 0.1$ (filled dots) the lifetime is only $0.14\,$s. To better see the difference of the lifetime for the two ellipticities we normalized L_z by its initial value L_0. For the lower ellipticity $L_0 = 2.2\hbar$ and for the higher ellipticity $1.6\hbar$.

condensate [37, 38]. When the thermal cloud is not rotating, theoretical [37] and experimental [33] studies show nonexponetial behavior. For a gas completely in the hydrodynamic regime it is expected that the decrease in L_z has an exponential form [16].

To measure the decay rate of the angular momentum we use the following procedure. After spinning up the gas as discussed in Sec. III, we slowly increase the static ellipticity within $10\,$ms, wait for a certain hold time to let the angular momentum partially decay and then we remove the ellipticity again within $10\,$ms. Finally we excite the radial quadrupole mode and observe the precession to determine L_z using the simplified procedure discussed earlier.

In Figure 4 we show two examples for the decay of L_z. We find that the decay of the angular momentum perfectly fits an exponential behavior for all the static ellipticities, temperatures, and interaction strengths we used. For the lowest temperatures obtained the lifetime for a gas in the unitarity limit goes up to $1.4\,$s, presumably limited by a residual anisotropy of the trap. This lifetime is by more than a factor of thousand larger then the radial trap oscillation period. Furthermore the lifetime of the angular momentum is much larger than the lifetime of collective excitation modes. For example the lifetime of the radial quadrupole mode under the same conditions is only $2\,$ms. A larger ellipticity of the trap significantly decreases the lifetime of L_z.

In the following we investigate quantitatively the dependence of the decay rate of the angular momentum, λ, on ellipticity and temperature. The experimental results are shown in Fig. 5 for two different temperatures.
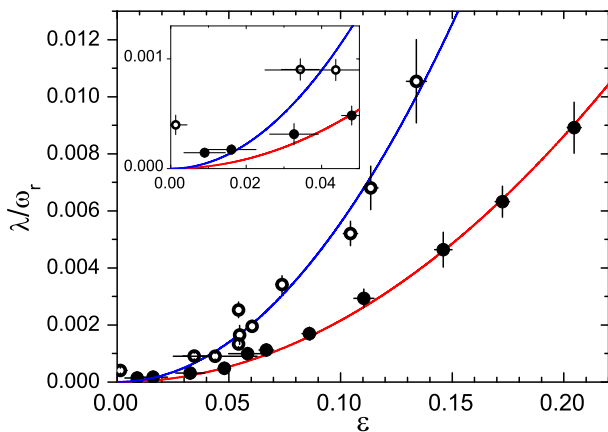
Figure 5: Normalized decay rate of the angular momentum as a function of the ellipticity for a gas in the unitarity limit. The temperatures are $T/T_F = 0.22(3)$ (filled dots) and $0.35(2)$ (open dots). The solid lines are fits based on the expected behavior for a Boltzmann gas [16]. The inset shows the low ellipticity region.

The full circles display the data for a temperature of $T/T_F = 0.22(3)$ and the open circles correspond to a temperature of $T/T_F = 0.35(2)$. For better comparison with theory we plot the normalized decay rate λ/ω_r. A strong increase of the decay rate with increasing ellipticity shows the important role of the trap anisotropy on the lifetime of the angular momentum. For both temperatures the qualitative behavior of the decay rate is the same.

Next we compare the behavior of the decay rate with a theoretical prediction for a Boltzmann gas [16]. As we showed recently in Ref. [11], a Boltzmann gas describes the behavior of a unitarity-limited gas in the normal state reasonably well. The predicted behavior of the decay rate is given by $\lambda/\omega_r = 2\epsilon^2 \omega_r \tau$ under the assumption that $\epsilon \ll 1/(4\omega_r \tau)$ [39], where τ is the relaxation time or effective collision time [11, 40, 41]. This condition is well fulfilled in our system because the gas is in the hydrodynamic regime where $\omega_r \tau \ll 1$. We compare this theoretical prediction, with τ as a free parameter, to our measurements. We find $\omega_r \tau = 0.108(5)$ for the lower temperature and $\omega_r \tau = 0.28(1)$ for the higher temperature data.

Note that at very low ellipticity, $\epsilon < 0.02$, the observed decay rate for both temperatures lies significantly above the expected behavior; see inset of Fig. 5. We attribute this to an additional anisotropy of the trap beyond simple ellipticity. This weak anisotropy becomes relevant only at very low ϵ. Furthermore the finite linear heating rate of the trapped gas of $0.05\,T_F\,\mathrm{s}^{-1}$ becomes important when the decay rate is very low, which means that the lifetime of L_z is on the order of seconds. In this case the temperature cannot be assumed to be constant during the decay of L_z.

A recent calculation of the relaxation time τ for a Fermi gas in the unitarity limit [11] allows us to com-

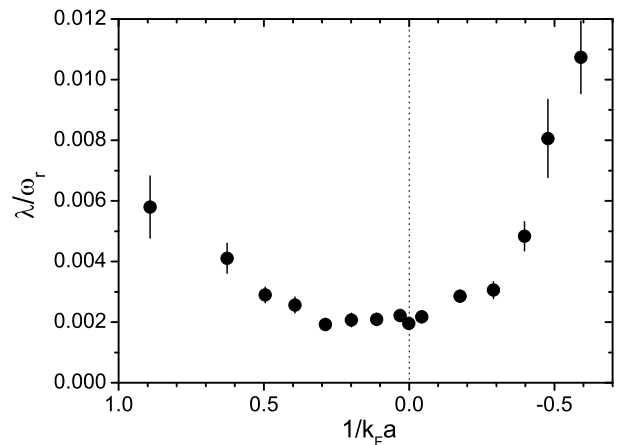Figure 6: Lifetime of the angular momentum versus interaction parameter $1/k_F a$ for $\epsilon = 0.09$. The temperature for $1/k_F a = 0$ is $T/T_F = 0.22(3)$.

pare the experimental values for $\omega_r \tau$ to theory. For $T/T_F = 0.35$ the obtained relaxation time of $\omega_r \tau = 0.28$ is clearly larger than the calculated value of $\omega_r \tau = 0.13$. This means that the theory predicts that the gas is somewhat deeper in the hydrodynamic regime compared to the experimental findings. Similar deviations showed up when the theory was compared to the temperature dependence of collective oscillations [11]. For the lower temperature the obtained value for $\omega_r \tau$ cannot be compared to the calculation of Ref. [11] as the theory is restricted to higher temperatures.

Finally we study the decay of the angular momentum in the crossover region between the BEC and BCS regimes. We measure the decay rate for different interaction parameters $1/k_F a$. The experimental sequence is the same as for the decay rate in the unitarity limit beside ramping the magnetic field to the desired value in $100\,\mathrm{ms}$ before increasing the ellipticity and ramping back the magnetic field in $100\,\mathrm{ms}$ before exciting the quadrupole mode. Here the magnetic field is changed slowly such that the gas is not collectively excited. The ellipticity for all magnetic fields is set to be $\epsilon = 0.09$. This sizeable value of ϵ ensures that a small anisotropy beyond ellipticity does not affect the decay rate and makes the measurement less sensitive to heating while the angular momentum damps out as discussed above.

Figure 6 shows the decay rate of the angular momentum as a function of the interaction strength. The lifetime is largest where the interaction is strongest and accordingly the relaxation time is short. In addition to the two-body interaction strength, pairing effects play an important role for the relaxation time [11]. This might explain the higher decay rates for $1/k_F a < 0$, where the pairing is weak, compared to the decay rates for $1/k_F a > 0$, where the atoms are bound to molecules. Similar behavior has been seen in [12] for the lifetime of a vortex lattice. Note that Ref. [12] also reports a decrease of the lifetime in a narrow region around $1/k_F a = 0$,

which we do not observe for our trap parameters.

In summary the hydrodynamic behavior in the crossover region leads to a very long lifetime of L_z.

V. CONCLUSION

In this work we have presented measurements on a strongly interacting Fermi gas carrying angular momentum. The angular momentum of the gas exhibits long lifetimes due to the deeply hydrodynamic behavior of the normal state in such a system. We investigated the decay rate of the angular momentum depending on the ellipticity of the trapping potential for two different temperatures. We find that the experimental results are in good agreement with the expected behavior for a simple Boltzmann gas. The dependence of the decay rate of the angular momentum on the interaction strength in the BEC-BCS crossover region confirms that collective motion is very stable as long as the interaction strength is sufficiently large.

The long lifetime of the angular momentum in a rotating strongly interacting Fermi gas allows us to further investigate rotational properties both in the superfluid and normal phase in detail and with high precision. Currently we investigate the moment of inertia of the gas for different temperatures [42].

Appendix A

To calculate the precession angle and the oscillation of the width we assume that the frequency and damping rate for the $m = \pm 2$ excitations are independent. For the damping of each excitation we assume a exponential behavior. A superposition of the two excitations results in the fit function for the precession angle [27]

$$
\begin{aligned}
&\tan\left(2(\phi - \phi_e)\right) = \\
&\frac{e^{-(\Gamma_+ - \Gamma_-)t}\sin\left(\omega_+ t + 2\phi_0\right) - \sin\left(\omega_- t + 2\phi_0\right)}{e^{-(\Gamma_+ - \Gamma_-)t}\cos\left(\omega_+ t + 2\phi_0\right) + \cos\left(\omega_- t + 2\phi_0\right)}
\end{aligned} \quad \text{(A1)}
$$

Here $\omega_{\pm}$ are the frequencies, $\Gamma_{\pm}$ are the damping rates, ϕ_0 is the initial angle for the two excitations and ϕ_e is the precession angle resulting from the expansion of the cloud. For the oscillation of the width difference ΔW we get

$$
\begin{aligned}
\Delta W^2 =\ & 4A e^{-(\Gamma_+ + \Gamma_-)t}\cos^2\left(\frac{(\omega_+ + \omega_-)}{2}t + 2\phi_0\right) \\
& + A(e^{-\Gamma_+ t} - e^{-\Gamma_- t})^2,
\end{aligned} \quad \text{(A2)}
$$

where A is the amplitude of the oscillation.

Appendix B

Here we calculate the effect of the expansion of the cloud on the precession angle. Assuming conservation of angular momentum during the expansion, the rotation frequency Ω of the gas decreases as the size of the cloud is increasing. We introduce an effective precession time t_e which accounts for the changing precession angle ϕ during expansion. The total change of the precession angle resulting from the expansion is given by

$$
\phi_e = \int_0^{t_{\text{TOF}}} \dot{\phi}(t)\,dt = \dot{\phi}(0)t_e, \quad \text{(B1)}
$$

where $\dot{\phi}(0)$ is the precession frequency when the gas is still trapped and t_{TOF} is the expansion time. Assuming that also during the expansion $\dot{\phi}(t) = L_z/(2M r_{\text{rms}}^2(t))$ is still valid and inserting this into Eq. B1 we get

$$
t_e = \int_0^{t_{\text{TOF}}} r_{\text{rms}}^2(0)/r_{\text{rms}}^2(t)\,dt. \quad \text{(B2)}
$$

To calculate the relative increase of the cloud size during expansion, $r_{\text{rms}}^2(t)/r_{\text{rms}}^2(0)$, we use the scaling approach; see e.g. [10]. For our experimental parameters, $\omega_r = 800\,\text{Hz}$ and $t_{\text{TOF}} = 0.8\,\text{ms}$, we get an effective precession time of $t_e = 0.26\,\text{ms}$. This is shorter than the typical precession time in the trap of $0.75\,\text{ms}$.

[1] M. Inguscio, W. Ketterle, and C. Salomon, eds., *Ultracold Fermi Gases* (IOS Press, Amsterdam, 2008), Proceedings of the International School of Physics "Enrico Fermi", Course CLXIV, Varenna, 20-30 June 2006.

[2] S. Giorgini, L. P. Pitaevskii, and S. Stringari, Rev. Mod. Phys. **80**, 1215 (2008).

[3] B. Clancy, L. Luo, and J. E. Thomas, Phys. Rev. Lett.

99, 140401 (2007).

[4] M. J. Wright, S. Riedl, A. Altmeyer, C. Kohstall, E. R. Sánchez Guajardo, J. Hecker Denschlag, and R. Grimm, Phys. Rev. Lett. **99**, 150403 (2007).

[5] M. Bartenstein, A. Altmeyer, S. Riedl, S. Jochim, C. Chin, J. Hecker Denschlag, and R. Grimm, Phys. Rev. Lett. **92**, 203201 (2004).

[6] J. Kinast, S. L. Hemmer, M. E. Gehm, A. Turlapov, and J. E. Thomas, Phys. Rev. Lett. **92**, 150402 (2004).

[7] J. Kinast, A. Turlapov, and J. E. Thomas, Phys. Rev. A **70**, 051401(R) (2004).

[8] J. Kinast, A. Turlapov, and J. E. Thomas, Phys. Rev. Lett. **94**, 170404 (2005).

[9] A. Altmeyer, S. Riedl, C. Kohstall, M. J. Wright, R. Geursen, M. Bartenstein, C. Chin, J. Hecker Denschlag, and R. Grimm, Phys. Rev. Lett. **98**, 040401 (2007).

[10] A. Altmeyer, S. Riedl, M. J. Wright, C. Kohstall, J. Hecker Denschlag, and R. Grimm, Phys. Rev. A **76**, 033610 (2007).

[11] S. Riedl, E. R. Sánchez Guajardo, C. Kohstall, A. Altmeyer, M. J. Wright, J. Hecker Denschlag, R. Grimm, G. M. Bruun, and H. Smith, Phys. Rev. A **78**, 053609 (2008).

[12] M. W. Zwierlein, J. R. Abo-Shaeer, A. Schirotzek, C. H. Schunck, and W. Ketterle, Nature **435**, 1047 (2005).

[13] F. Chevy, K. M. Madison, and J. Dalibard, Phys. Rev. Lett. **85**, 2223 (2000).

[14] P. C. Haljan, B. P. Anderson, I. Coddington, and E. A. Cornell, Phys. Rev. Lett. **86**, 2922 (2001).

[15] A. E. Leanhardt, A. Görlitz, A. P. Chikkatur, D. Kielpinski, Y. Shin, D. E. Pritchard, and W. Ketterle, Phys. Rev. Lett. **89**, 190403 (2002).

[16] D. Guèry-Odelin, Phys. Rev. A **62**, 033607 (2000).

[17] S. Jochim, M. Bartenstein, A. Altmeyer, G. Hendl, S. Riedl, C. Chin, J. Hecker Denschlag, and R. Grimm, Science **302**, 2101 (2003).

[18] M. Bartenstein, A. Altmeyer, S. Riedl, R. Geursen, S. Jochim, C. Chin, J. Hecker Denschlag, R. Grimm, A. Simoni, E. Tiesinga, C. J. Williams, and P. S. Julienne, Phys. Rev. Lett. **94**, 103201 (2005).

[19] $\epsilon' = (\omega_x'^2 - \omega_y'^2)/(\omega_x'^2 + \omega_y'^2)$, where ω_x' and ω_y' are the trap frequencies in the frame of the rotating potential.

[20] F. Chevy and S. Stringari, Phys. Rev. A **68**, 053601 (2003).

[21] S. Sinha, Phys. Rev. A **55**, 4325 (1997).

[22] R. J. Dodd, K. Burnett, M. Edwards, and C. Clark, Phys. Rev. A **56**, 587 (1997).

[23] A. A. Svidzinsky and A. L. Fetter, Phys. Rev. A **58**, 3168 (1998).

[24] F. Zambelli and S. Stringari, Phys. Rev. Lett. **81**, 1754 (1998).

[25] We determine $r_{\rm rms}$ at unitarity from the trap parameters using $E_F = 2M\omega_r^2 r_{\rm rms}^2 \sqrt{1+\beta}$ where we used the universal scaling parameter $\beta = -0.56$ [2]. Note that this underestimates $r_{\rm rms}$ by a few percent because it does not take into account the finite temperature and the rotation of the gas. This does not affect the measurement of the lifetime of rotation as this depends on the relative change of L_z.

[26] For the parameters used in the experiment a zero temperature Thomas-Fermi profile fits the density distribution reasonably well.

[27] V. Bretin, P. Rosenbusch, F. Chevy, G. V. Shlyapnikov, and J. Dalibard, Phys. Rev. Lett. **90**, 100403 (2003).

[28] J. E. Williams, E. Zaremba, B. Jackson, T. Nikuni, and A. Griffin, Phys. Rev. Lett. **88**, 070401 (2002).

[29] Note that the frequency of quadrupole mode oscillation ω_q depends on the rotation frequency of the gas via $\omega_q^2 = 2\omega_r^2 - \Omega^2$. This leads to a tiny shift of the maxima of ΔW^2 but does not affect our measurement of L_z within our experimental uncertainty.

[30] This is the largest magnetic field where absorption images can be taken with our current experimental setup.

[31] L. Luo, B. Clancy, J. Joseph, J. Kinast, and J. E. Thomas, Phys. Rev. Lett. **98**, 080402 (2007).

[32] Q. Chen, J. Stajic, and K. Levin, Phys. Rev. Lett. **95**, 260405 (2005).

[33] K. W. Madison, F. Chevy, W. Wohlleben, and J. Dalibard, Phys. Rev. Lett. **84**, 806 (2000).

[34] K. W. Madison, F. Chevy, V. Bretin, and J. Dalibard, Phys. Rev. Lett. **86**, 4443 (2001).

[35] E. Hodby, G. Hechenblaikner, S. A. Hopkins, O. M. Maragò, and C. J. Foot, Phys. Rev. Lett. **88**, 010405 (2002).

[36] To estimate the increase of the temperature through the decay of the rotation we assume that the rotation energy is completely converted into heat. In the experiments L_z is well below $3\hbar$ which leads to a relative temperature increase of $\Delta T/T < 0.02$ in the relevant temperature range. This is clearly below the uncertainty of our temperature measurement.

[37] O. N. Zhuravlev, A. E. Muryshev, and P. O. Fedichev, Phys. Rev. A **64**, 053601 (2001).

[38] J. R. Abo-Shaeer, C. Raman, and W. Ketterle, Phys. Rev. Lett. **88**, 070409 (2002).

[39] For the temperatures used in the measurements $1/(4\omega_r\tau) > 0.9$ for a gas in the unitarity limit.

[40] L. Vichi, J. Low. Temp. Phys. **121**, 177 (2000).

[41] K. Huang, ed., *Statistical Mechanics* (John Wiley & Sons, New York, 1987), page 104.

[42] S. Riedl *et al.*, in preparation.